Transferring electrochemical reduction of CO_2 from semi-batch into continuous mode of operation using gas diffusion electrodes

D. Kopljar[1], N. Wagner[2], E. Klemm[1]

1: University of Stuttgart, Institute for Chemical Technology,
Pfaffenwaldring 55, 70569 Stuttgart, Germany
2: German Aerospace Center (DLR), Institute of Engineering Thermodynamics,
Pfaffenwaldring 38-40, 70569 Stuttgart, Germany

* Corresponding author:
Dennis Kopljar
dennis.kopljar@itc.uni-stuttgart.de
phone: 0049-711-685 60009

Abstract

The electrochemical reduction of CO_2 is a promising method for its conversion which still suffers from important challenges that have to be solved before industrial realization becomes attractive. This study describes the optimization of gas diffusion electrodes with respect to catalyst dispersion and mass transport limitations allowing solubility issues to be circumvented and current densities to be increased to industrially relevant values. Consequently, the transfer of the promising results from semi-batch experiments into continuous mode of operation is demonstrated, and it is shown how the energetic efficiency can be significantly improved by the choice of electrolyte, in terms of concentration and type. Thereby ohmic losses can be decreased and the intrinsic activity improved.

Short text for the Tab. of contents section

Electrochemical reduction is an attractive pathway for its substantial utilization. This article describes how the important requirements of technical realization, namely high reaction rates, continuous operation and energetic efficiency are approached using gas diffusion electrodes loaded with electrocatalyst-nanoparticles, a microstructured flow-cell and electrolyte optimization.
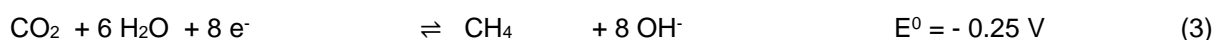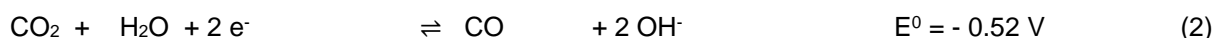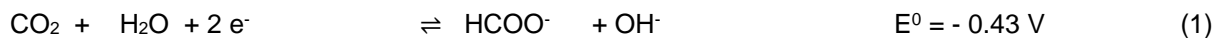
Keywords.
Electrocatalysis, CO_2 reduction, gas diffusion electrodes, formate/ formic acid
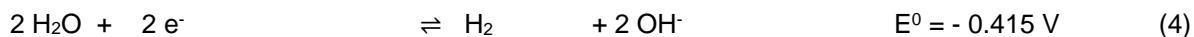
1. **Introduction**

Nowadays, it is hard to imagine a life without the benefits and achievements the fossil age has brought us. The abundance of cheap oil, natural gas and coal ensured a seemingly never-ending source of inexpensive energy and chemical feedstock for the production of a vast variety of carbon-based chemicals [1]. However, after more than a century of their use, the downside of this heavy dependency becomes increasingly obvious in terms of both ecological and economical aspects. Furthermore, it is now mainly agreed upon that the emission of CO_2 and its accumulation in the atmosphere contributes to anthropogenic climate change which is why the international community has started to increase and coordinate their efforts to decrease CO_2 output and attenuate global warming.

Specific measures are manifold and it is clear that this can only be achieved by shifting global energy generation as well as chemical production away from fossil towards renewable and alternative resources [2,3]. In this respect, CO_2, is an attractive feedstock as it can be gathered as by-product in many chemical processes but also in reactions encountered in biorefineries such as biogas production or ethanol fermentation. Hence, it is abundant and cheap (depending on concentration and effort for purification) while its capturing and processing constitutes the possibility of turning a waste material into value [4,5].

One method to valorize CO_2 is its electrochemical reduction to small organic compounds on the cathode side of an electrochemical cell. Depending on the electrode material, different products can be produced, mainly formic acid/ formate, CO, methane but also other small hydrocarbons [6,7]. Some examples with their corresponding standard potential [8] at 25 °C and neutral aqueous media at pH = 7 are given here:

$$CO_2 + H_2O + 2\,e^- \quad \rightleftharpoons \quad HCOO^- + OH^- \qquad E^0 = -0.43\ V \qquad (1)$$
$$CO_2 + H_2O + 2\,e^- \quad \rightleftharpoons \quad CO + 2\,OH^- \qquad E^0 = -0.52\ V \qquad (2)$$
$$CO_2 + 6\,H_2O + 8\,e^- \quad \rightleftharpoons \quad CH_4 + 8\,OH^- \qquad E^0 = -0.25\ V \qquad (3)$$

Furthermore, when aqueous electrolyte is used, an important side reaction is hydrogen evolution (HER) (eq. 4) which occurs in the same potential range and can make up a considerable fraction of the consumed charge.

$$2\,H_2O + 2\,e^- \quad \rightleftharpoons \quad H_2 + 2\,OH^- \qquad E^0 = -0.415\ V \qquad (4)$$

Although the actual product distribution is dependent on reaction conditions and usually a mixture of products is obtained, the metals can be classified according to their main product in aqueous electrolyte with Sn, Pb, Hg, In (or their corresponding oxides) producing formate [9]. Its electrochemical production could be an attractive pathway, as it is considered to be competitive in terms of sustainability and economics compared to its conventional production [10,11] and because it can be used to store electricity in chemical form. In turn, formic acid can serve as hydrogen storage chemical which is easily decomposed at room temperature releasing hydrogen or be fed into direct-formic acid fuel cells [12,13].

With the above mentioned catalysts, production of formate could already be demonstrated with selectivity >80%. However, some challenges have to be solved before its technical application becomes interesting in an industrial scale: (i) the derivation of more active catalysts to decrease the high activation barriers responsible for high overpotentials, (ii) the requirement of much higher production rates towards the desired product and (iii) the demonstration of its continuous production which combines the above with low ohmic losses and long-term stability as well as incorporation of a suitable anode reaction (usually oxygen evolution or hydrogen oxidation) [8,14,15].

To solve these challenges, a substantial amount of work has been conducted in the last years which has led to remarkable advances in the optimization of the process and understanding of the reaction [7,16,17]. Especially the progress made in the design of nanostructured [18–21], metal oxide/oxide-derived [22] or novel catalysts [23,24] is promising and, together with in-situ investigations [25,26] has allowed for the deepening of the available knowledge by elucidating active sites and revealing mechanistic aspects. However, for technical realization, high yields - characterized by high current density (CD, linked to reaction rate by Faraday's law) and Faradaic efficiency (FE, percentage of current going into desired product) - are mandatory and CDs on the order of 100-500 $mA \cdot cm^{-2}$ or even 1000 $mA \cdot cm^{-2}$ as recently suggested have to be aimed at [27]. Low solubility of CO_2 in aqueous electrolyte, on the other hand, limits the achievable current density on flat electrodes to below 10 $mA \cdot cm^{-2}$ [11,27]. At higher CD diffusion of CO_2 to the active site becomes rate-determining and HER increasingly proceeds. In this respect, the use of gas diffusion electrodes (GDE), originating from fuel cell technology, has been shown to allow for shifting limitations to much higher CD. Commonly used GDEs are porous electrodes comprised of a carbon matrix wherein the catalyst is dispersed. The binding agent, usually PTFE, besides ensuring mechanical stability, renders the surface hydrophobic, whereby CO_2 can be fed in the gas phase from one side while the electrolyte penetrates into the pore network from the other. Consequently, the triple-phase boundary between gas, electrolyte and catalyst where reaction takes place forms in the interior of the electrode and can be massively enhanced due to the high surface area of the support. The success of this approach has been demonstrated in several publications [28–31], amongst others in our previous articles [32,33]. Although the use of GDEs has shown to be indispensable and the potential of their optimization has been proven to be highly beneficial in other applications such as fuel cells or water electrolysis, more profound studies that focus on their preparation, characterization and optimization for CO_2 reduction are still scarce [34–36].

In this work, we want to show that the previously reported performance of gas diffusion electrodes prepared by a newly developed dry deposition technique can be transferred into continuous mode of operation. As a starting point, the results from our previous article will be shortly summarized and extended by further results, before the important parameters for continuous operation are examined and optimized to obtain high current density at improved energetic efficiency.

2. Experimental

2.1 Electrode preparation

GDEs have been prepared *via* a newly developed and simple dry deposition method described in [33]. In short, the components are thoroughly mixed in a knife mill (IKA, M20 Universal mil), put in a cylindrical mask of 12.56 cm² and pressed with a pressure of 11 kN·cm^{-2}. The GDE is sintered in an oven at 340 °C, slightly above the melting point of PTFE for 10 min in N_2 atmosphere. The GDEs are comprised of acetylene black (Alfa Aesar, 99.9%) and PTFE (Dyneon, TF 92070Z) in a ratio of 65:35. The active metal tin is either mechanically mixed using commercial Sn-nanopowder (Sigma-Aldrich, <150 nm, >99% trace metal basis) with a loading of 1 mg·cm^{-2} or supported on the carbon black beforehand. On the anode side a commercial catalyst-coated membrane (Ion-Power, Nafion NR-212, 50 µm thickness, coated with Pt/C, 0.5 mg Pt·cm^{-2}) was employed.

2.2 Catalyst synthesis

The carbon-supported SnO_2 electrocatalyst is synthesized by a homogenous precipitation method, introduced by [37]. As precursor solution $SnCl_2$ is mixed with urea in aqueous solution, carbon black added and sonicated for one hour and mixed for 4 hours. The slurry was then refluxed at 90 °C for 4 h through which urea slowly decomposed, the pH-value is homogenously increased resulting in precipitation of tin oxide (SnOx) on the carbon surface. Actual tin mass has been quantified by burning off the carbon at 1000 °C and weighing the residue. The 1.81 wt.-% gives an actual GDE metal loading of 0.87 mg·cm^{-2}.

2.3 Electrochemical reactor and experimental procedure

Semi-batch experiments were conducted in a custom-made cell made from PMMA consisting of cathode and anode chamber separated by a proton-conducting membrane (Nafion® 117, DuPont). A scheme and more details on the experimental procedure are given in [33]. The experiments were conducted in galvanostatic mode with a potentiostat (Gamry Reference3000), a Pt-foil counter electrode and a Hg|HgO reference electrode filled with 1M KOH (E = 98 mV vs. SHE at pH 14 and 25 °C). The experiments in continuous mode of operation were performed using a self-developed microstructured electrochemical flow-cell made from PMMA (PEEK for KOH-experiments), a scheme of the setup is shown in Fig. 1. CO_2 (Westfalen, 5.9) was continuously fed on the cathode side at a flow-rate of 8 mL/min, hydrogen was fed on the anode side. The electrolyte ($KHCO_3$: 0.1 M or 1.0 M> 99.99% trace metal basis; KOH: puriss, p.a.; water: HPLC-grade; all Sigma-Aldrich) was pumped using a two-piston pump at a flow-rate of 1.0 mL/min. The $KHCO_3$ electrolyte was adjusted to pH = 10 as this was shown to be advantageous in our previous article and in literature [25,38]. The electrolyte was pre-electrolyzed for 2 h at 2 V to minimize contamination of the electrode surface by impurities and metal traces. When noted, iR-compensation was performed using Current-Interrupt technique automatically done by the Gamry software between each data point.

2.4 Analytics and characterization

The amount of formate produced was quantified using high performance liquid chromatography with an Agilent Technology type 1200 equipped with a Nucleogel Sugar 810H column (Macherey–Nagel) and an RI detector. To evaluate gas phase composition, gas chromatography was used on an Agilent Technologies 7890. Samples were injected through a Poropak Q and Molsieve 5A connected to the TCD. Combining both GC and HPLC, the current balance could be closed in between 5% for all experiments. At high current density (>250 mA·cm^{-2}), formate concentration is high enough for formate to diffuse through the membrane to the anode side where it is readily oxidized, as described by other authors [39]. A quantitative assessment of formate production is not possible anymore. As this is not an intrinsic problem of the process (concentrations in continuous mode much smaller due to low residence time) but rather an issue of analysis, reaction was stopped after 0.5 h to quantify formate concentration. Gas product analysis shows that besides a small shift from formate to CO (see below), FE stays nearly constant over 1 h.

2.5 Characterization

In order to evaluate dispersion of the catalyst, scanning electron microscopy (SEM) images have been taken at the DLR with a Zeiss ULTRA plus microscope equipped with an AsB (angle selective backscattered electron) detector to obtain material contrast images. X-ray Photoelectron Spectroscopy (XPS) has been performed by Pawel Gazdzicki from the DLR using a Thermo ESCALAB 250 (Thermo Electron Corporation) ultra-high vacuum facility with a base pressure of 1×10^{-9} mbar. Analysis was conducted using a nonmonochromated AlKa X-ray source (Thermo XR4) operated at 300W in combination with a hemispherical six channeltron electron energy analyzer operated in small area mode (0.8mm^2 analyzed surface area). The concentrations of elements were quantified using sensitivity factors provided by Thermo Scientific using Shirley algorithm for peak background correction.
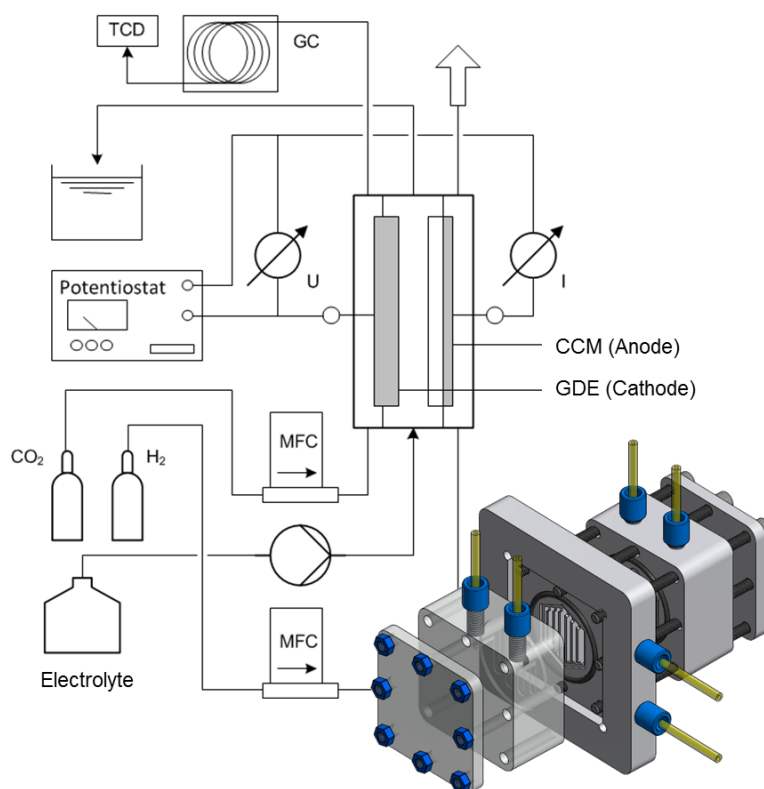
Fig. 1. Experimental setup for continuous CO_2 reduction and H_2 oxidation

3. **Results**

Results from semi-batch experiments and use of carbon-supported SnO₂ nanoparticles

This study is based on the results from a previous article where the importance of the preparation procedure and the optimization of the so prepared gas diffusion electrode (GDE) for CO_2 reduction has been demonstrated [33]. The development of a dry deposition technique for their preparation has been reported, which produces GDEs that allow CO_2 reduction towards formate up to a current density (CD) of 200 mA·cm⁻². For stability reasons in the pressing step, a small portion of graphite has been added to the powder mixture what decreases brittleness of the samples, yet, due to its non-porous nature and lack of superordinate pore structure contrary to carbon black, it is barely suitable for efficient gas transport and, consequently, as component of GDEs. Compared to our previous article, graphite was left out and the metal loading decreased from 5 to 1 mg·cm⁻², both effecting performance (see below).

The ability to efficiently facilitate the transport of CO_2 to the active sites, can be evaluated by performing galvanostatic experiments at different CDs and analyzing product distribution. The CD at which mass transport limitation gradually sets in is characterized by an increase HER compensating for missing CO_2. The results are illustrated in Fig. 2. The electrolyte employed was 0.1 M KHCO₃, adjusted with KOH to a pH-value of 10 which has been shown to be advantageous in a former study what is supported by recent

findings [25,38]. The FE for CO_2 reduction (CO + formate) stays at around 90% up to 200 mA·cm^{-2} beyond which it gradually decreases in favor of HER.
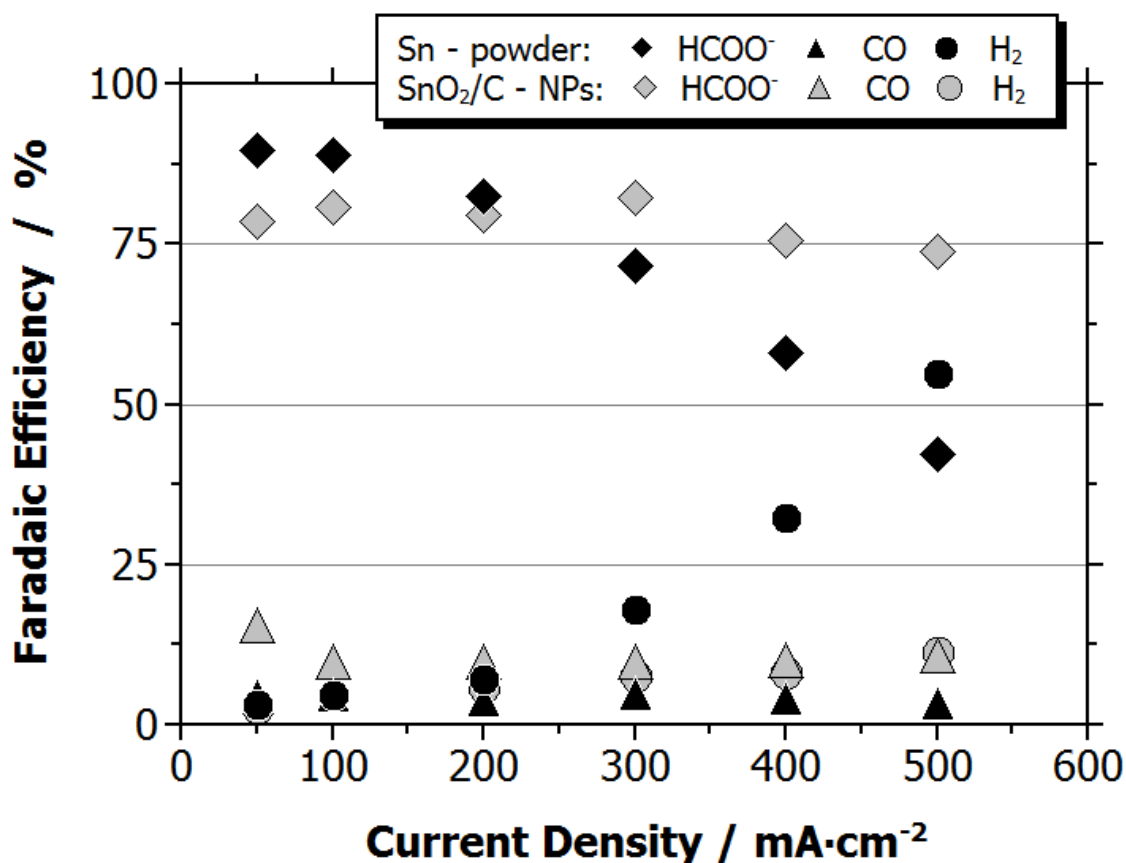

Fig. 2. Product distribution over applied current density for GDEs made from commercial Sn-powder- and SnO_2/C.

The results are very promising already, yet, the disadvantage of the mechanical mixing of the Sn-powder is the occurrence of highly agglomerated tin clusters up to several μm (image in [33]). This results in bad catalyst utilization and low activity. To improve dispersion, carbon-supported tin oxide nanoparticles (SnO_2/C in the following) have been synthesized through a simple homogeneous precipitation method. Consequently, finely dispersed nanoparticles with size around 10 nm and negligible agglomeration have been obtained, as evidenced by scanning electron microscopy (Fig. 3). The corresponding weight percentage of Sn on carbon was 1.81%, the metal loading of the prepared GDEs was 0.87 mg·cm^{-2}. A higher Sn to carbon ratio resulted in more pronounced agglomeration on the low surface-area support (Acetylene black, 75 m²/g). Therefore, a low metal loading has been chosen for the investigation, even though increasing loading has been shown beneficial for both activity (more active sites) and mass transport (lower diffusion length), yet, with the drawback of decreasing formate FE in favor of CO. The latter occurs due to the higher activity with increasing loading what makes less negative electrode potentials necessary for a given CD. This slightly shifts CO_2 reduction from formate to CO [33,40]. The same effect is responsible for the lower formate FE in the non-transport limited region using SnO_2/C nanoparticles compared to the

commercial powder (~ 80 to 90%). For a meaningful comparison, the same loading has been employed for the Sn-powder GDEs what results in slightly lower performance as compared to the previous results, what is, however, mostly compensated by the omission of the non-porous graphite. XPS data shown in Fig. 4 reveals the fully oxidic nature of the nanoparticle surface with no apparent peaks for metallic Sn (see in-lay for Sn3d region). Due to the low loading combined with the small particle size, XRD fails to show any Sn-specific reflexes. However, the diffractogram of the GDE with the Sn-powder before and after sintering shows how the sintering step leaves the Sn-particles fully oxidized. For both catalysts this is an important observation since the importance of the SnO_x-layer, was suggested by several recent studies to play a pivotal role in the reaction for different formate-producing catalysts [41–43].

The so produced SnO_2/C GDEs have been evaluated again in the same set of experiments, and the results are depicted in Fig. 2. Interestingly, it is shown that mass transport can be tremendously enhanced. This is because diffusion length to the active sites through the thin electrolyte layers covering the pore walls is greatly decreased. The CD can be increased up to 400 mA·cm^{-2} before mass transport limitation sets in and HER makes up more than 10% what is almost a 2-fold increase compared to our previous article and one of the highest reported literature values. Also activity is higher what in turn results in more CO production at moderate CDs. Besides the shown products, also small amounts of methane (<3%) is produced at all conditions on both GDEs. This work is not supposed to go into more detail on the further GDE and catalyst optimization but instead give the starting point from which the results were transferred into continuous mode of operation.
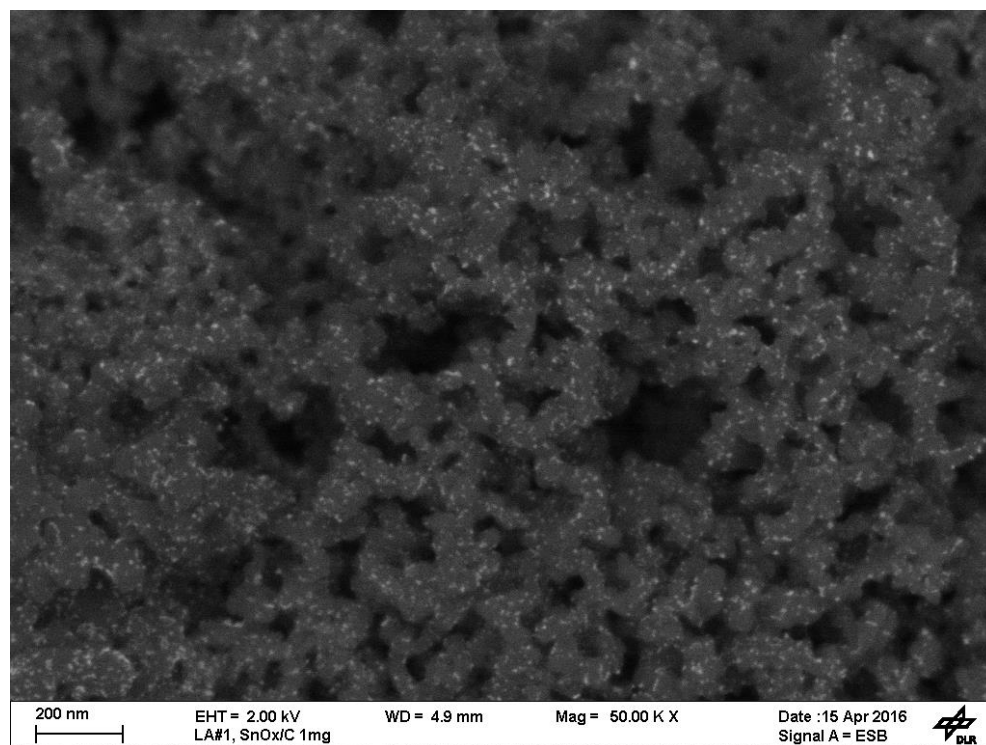

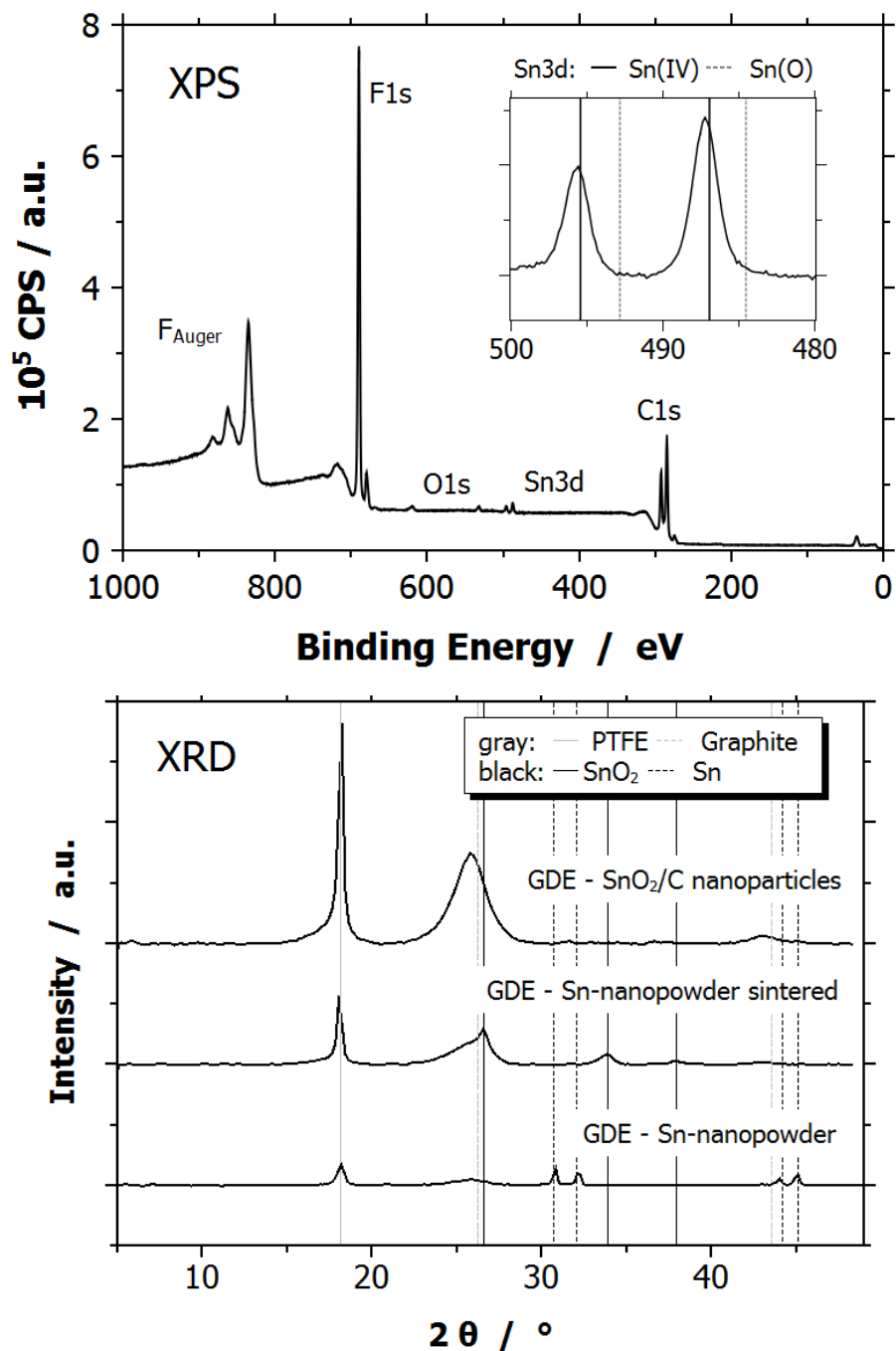Fig. 3. Scanning electron microscopy image of synthesized SnO_2/C, Sn weight-percentage of 1.81%

Fig. 4. XPS spectra of SnO₂/C GDE and XRD diffractogram of SnO₂- and powder-GDEs.

Performance in the continuous reactor setup

For the experiments in the continuous reactor setup a self-developed flow-cell with microstructured flow channels was utilized with the GDE on the cathode and hydrogen oxidation (HOR) taking place on the anode side on a commercial catalyst-coated membrane (CCM, Pt/C). HOR was chosen due to the simplicity of its

incorporation with the possibility of using commercial CCM but also because of its facile kinetics. Accordingly, observed overpotential can be ascribed to cathode polarization as the kinetic barriers for HOR are negligible at the employed CD [27]. As first step to study performance, experiments at fixed reactor voltage were conducted to evaluate time and voltage-current behavior. The results are presented in Fig. 5. Obviously, with increasing reactor voltage, CD goes up, here from 30 $mA \cdot cm^{-2}$ at 3 V to about 120 $mA \cdot cm^{-2}$ at 6 V. It is also evident that the GDE gets increasingly active with time which can be attributed to a progressive wetting of the electrode surface and increasing participation of catalyst in the reaction. This induction period is known from literature and explained by the loss of hydrophobicity due to decomposition of excess PTFE whereby electrolyte can penetrate deeper into the electrode pore-system [44].

For the experiments, also the product distribution was evaluated. The FE over time for formate and CO is depicted in Fig. 6 for different reactor voltages. H_2 has been left out to not overload the graph, its value maintained below 5% for all data points. For comparison with the semi-batch experiments, the FE for the first hour and after three hours has been taken and depicted over the corresponding CD. Besides the very good agreement, in both figures further observations known from semi-batch experiments can be made. As one can see, the ratio of FE towards formate and CO depends on both time and current which both can be attributed to a potential-induced shift from formate to CO generation (overall CO_2 reduction stays constant) when decreasing the electrode potential [33]. For low CD, a lower electrode potential is obvious. The time behavior comes from growing activity over time: with time the fraction of electrode surface participating in the reaction increases. As consequence, the (macroscopic) CD increases sharply. Although the reactor voltage is constant, the electrode potential is still subject to change because as CD increases the ohmic voltage drop which makes up a huge fraction of the voltage increases proportionally to the current. Its share as part of the reactor voltage grows what results in a corresponding decrease of electrode potential. This partially compensates the gain in activity which would otherwise be more pronounced if electrode potential stayed constant. In turn, CD increases slower, becomes almost stationary after 2 hours, but the continuing decrease of potential shifts CO_2 reduction slowly from formate to CO. To show that this is true, the result of an experiment with constant electrode potential (iR-compensated reactor voltage) of 1.3 V is included in the diagram. Indeed, the product distribution stays constant over time.
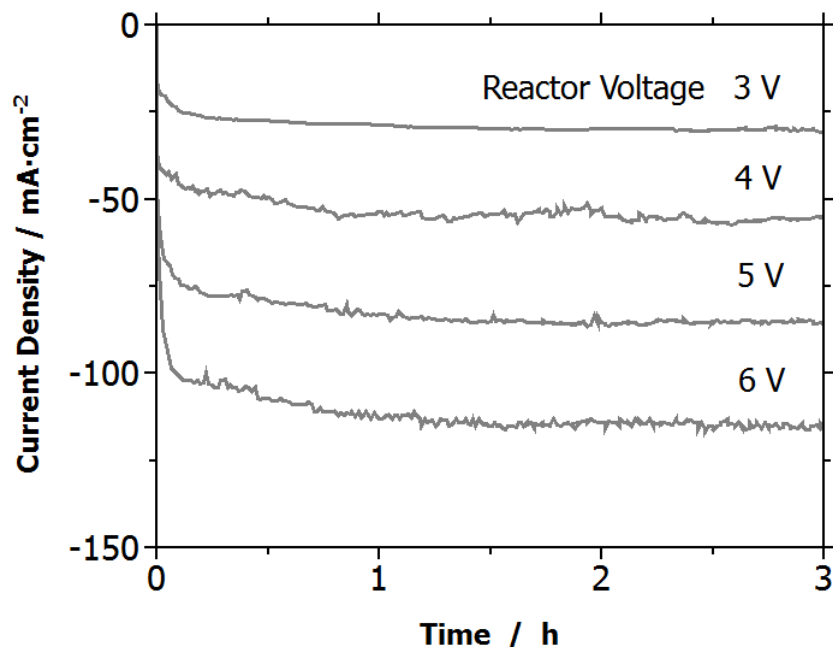
Fig. 5. Current density over time for different applied reactor voltages.

Reactor voltage and energetic efficiency

The favorable product distribution at relatively high CD proves the transfer to continuous operation successful, yet, it does not allow an assessment on energetic efficiency (EE) defined as the ratio of standard potential given by thermodynamics and the actual cell voltage, multiplied by the FE:

$$EE = \frac{E_{cell}^0}{E_{cell,actual}} \, FE \tag{5}$$

Here, this is CO_2 reduction to formate at pH = 10, 0.61 V vs. SHE, and hydrogen oxidation in acidic media (Nafion membrane), 0 V vs. SHE by definition. Due to the high barrier of CO_2 activation, achieving both high CD and EE above 50% is still a challenge, even though notable efforts have been made [45,46]. Without optimization, also in our case EE is *very* low. The current-voltage behavior, recorded via linear-sweep voltammetry (LSV) at 10 mV/s is illustrated in Fig. 7. Using the conditions from above (0.1 M $KHCO_3$ and pH = 10), the reaction starts at an overpotential of around 400 mV corresponding to a reactor voltage of around 1.0 V. However, the reactor voltage becomes substantial already at moderate rates. For a CD of 50 mA·cm^{-2} a reactor voltage of 4 V, for 100 mA·cm^{-2} ~ 5.5 V is needed, what corresponds to an EE of 13% and below 10%, respectively. The small deviations between the potentiostatic experiments and the LSV are due to the conditioning of the GDE before the scans (1.4 V iR-compensated for 1 h) which influences wetting and activity. Although $KHCO_3$ is a prevalently used electrolyte showing good results for CO_2 reduction [47,48], this does not take into account considerations on the EE in a full electrochemical cell for which besides its influence on the reaction itself also conductivity is crucial. This holds especially true for the concentration range usually used in half-cell experiments in literature (mostly between 0.1 M and 0.5 M).
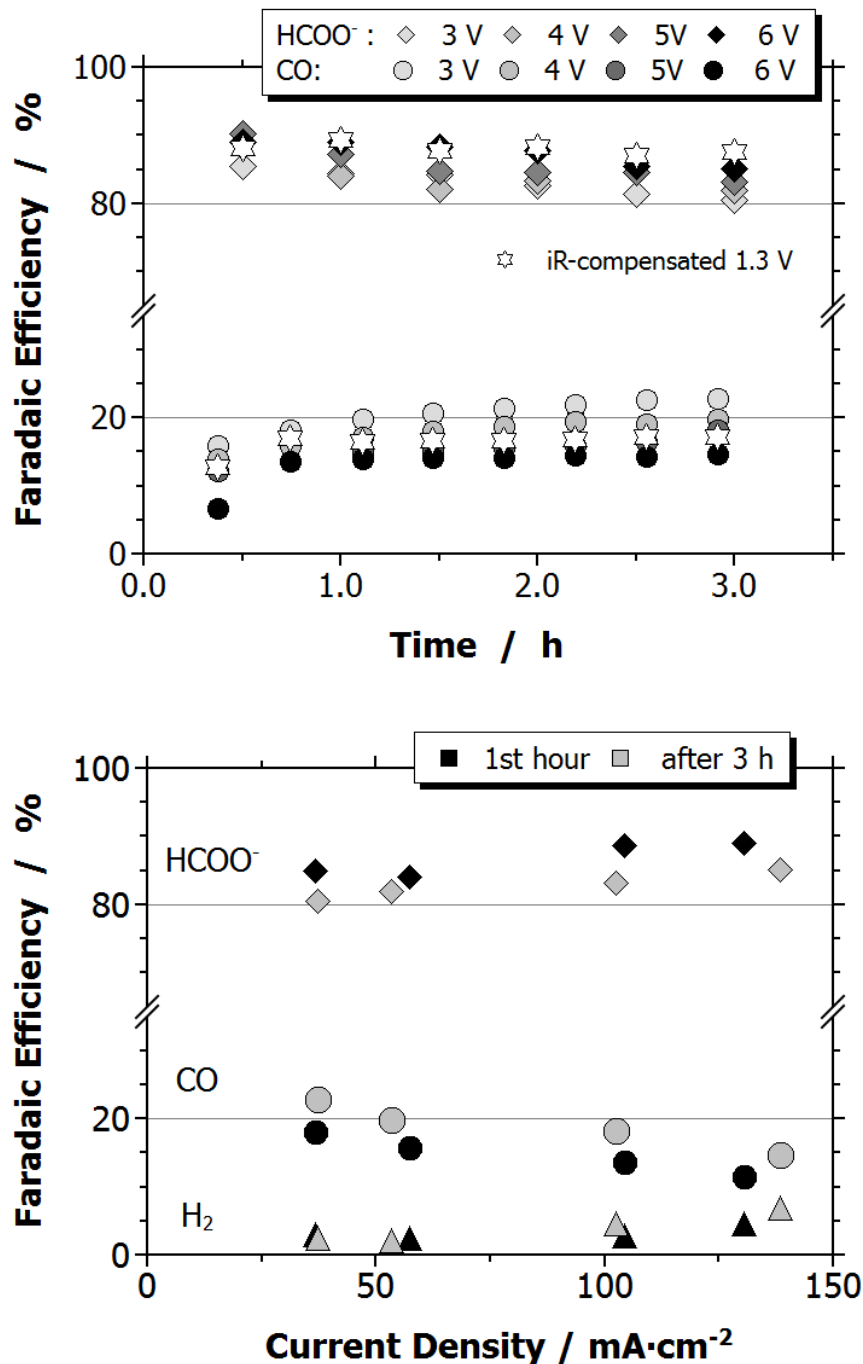
Fig. 6. Product distribution over a) time for different voltages and b) current density using 0.1 M KHCO₃

On the other hand, in a full electrochemical cell, EE including the ohmic voltage drop which depends on ionic conductivity of the electrolyte and the distance between the electrodes (4 mm in our case) becomes increasingly important, especially at high CD. The magnitude of this contribution to the reactor voltage can be assessed when iR-compensation is performed during LSV. As comparison of Fig. 7 a) and b) shows, ohmic contribution makes up a huge fraction of the reactor voltage, whereas actual electrode potential is

much lower, *e.g.* 1.5 V compared to 5 V reactor voltage at 100 mA·cm⁻². The electrolyte-related voltage drop can be minimized, either by decreasing electrode gap or increasing its conductivity, *e.g.* by increasing the concentration. Other important contributions to the ohmic losses are bubble accumulation between the electrodes (HER), limited conductivity of electrodes and contact resistances between components. As shown in Fig. 7, increasing $KHCO_3$ concentration to 1 M (still at pH = 10) results in a substantial decrease of cell voltage, from which a substantial part is due to the higher conductivity, 9.7 mS·cm⁻¹ vs. 75 mS·cm⁻¹. Product distribution is not noticeably affected and stays above 80% in the investigated potential range (see Tab. 1), whereas the iR-compensated scans show that also intrinsic activity improves. The influence of electrolyte type and its concentration has been described in a recent article which came to the same conclusion for Ag-based GDEs and CO production [49]. Therein, the increased activity is explained by the higher concentration of cations in the electrical double layer close to the electrode surface which helps stabilizing the reaction intermediate CO_2^-. Since the use of KOH as electrolyte was suggested to be beneficial for CO_2 reduction [45,49], as a next step the electrolyte was changed to 1 M KOH and the experiments repeated with the results depicted in the above Figures and in Tab. 1.
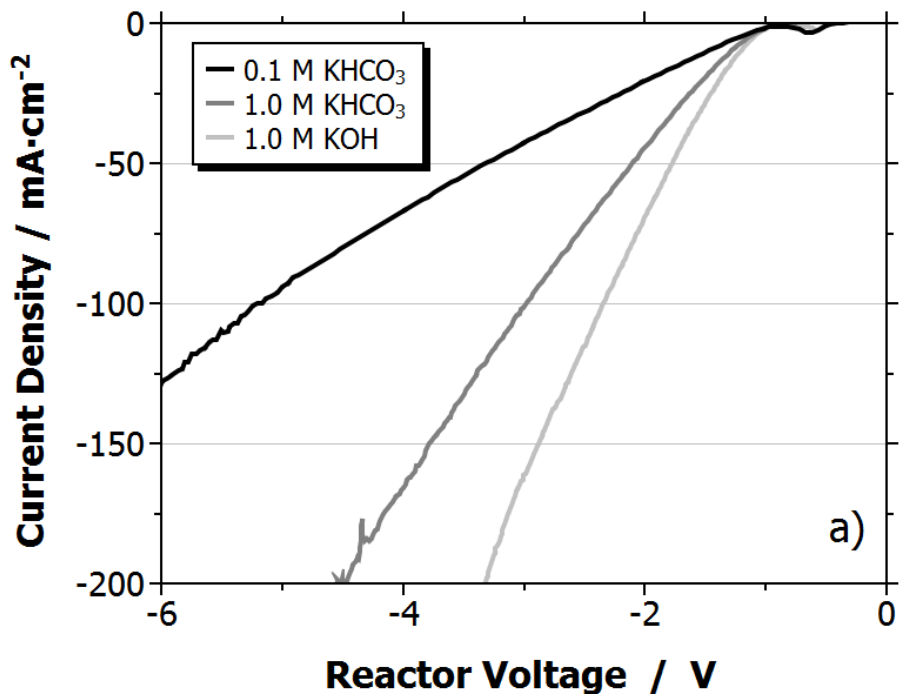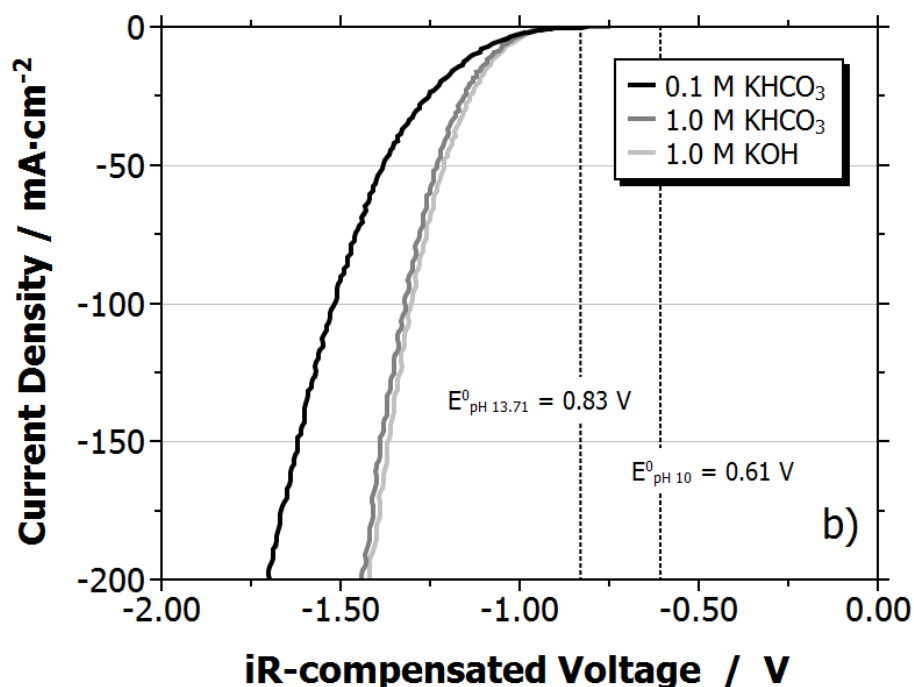
Fig. 7. Current density versus a) reactor voltage and b) iR-compensated voltage (electrode potential) for different electrolytes

Indeed, both in terms of reactor voltage (conductivity: 170 mS·cm^{-1}) and the intrinsic activity, a further improvement could be achieved, as suggested. Although the potential-current curve is very similar for KHCO$_3$ and KOH, one has to keep in mind the different pH values, resulting in different standard potentials. Accordingly, as E^0 for KOH is more negative, -0.83 V vs. SHE for pH 13.71 compared to -0.61 V for pH 10, the corresponding overpotential for reaction decreases from ~400 to 200 mV. Also the product distribution is still favorable, with ~80% formate. Finally, to see the overall improvement of this approach, experiments have been run at constant reactor voltage from 1.5 V to 2.5 V with KOH for three hours. The results are depicted in Fig. 8 and summarized in Tab. 1. Again, the same observations can be made concerning product distribution and the time behavior. The necessary reactor voltage, however, is much lower: a voltage of 2.5 V is now enough to drive the reaction at a notable rate of ~130 mA·cm^{-2} with a FE towards formate of 80%. Although this is an advancement from the results we started with, this still corresponds to an EE of only ~30%. Whereas, at 1.5 V and a CD of 20 mA·cm^{-2} the EE is at 45%, its decline goes relatively sharp with increasing reaction rate.

Tab. 1. Current density, product distribution and EE for different electrolytes at constant electrode potential or reactor voltage

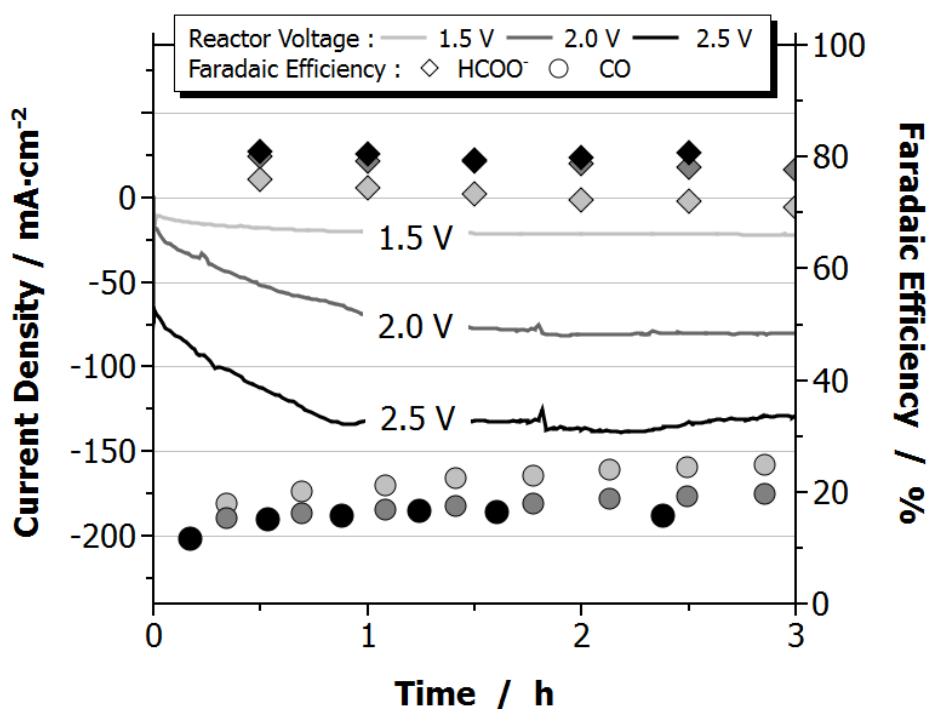| Electrolyte	$E_{iR-comp.}$ / V	$i_{\sim1h}$ / mA·cm^{-2}	FE (HCOO$^-$) / %	FE (CO) / %	FE (H$_2$) / %	$E_{reactor}$ / V	EE / %
1 M KHCO$_3$	1.30	83	80	16	3	3.48	14
	1.40	172	84	13	5	4.67	11
1 M KOH	1.30	116	79	15	5	2.51	26
	1.40	196	83	13	7	3.08	22
	-	21	74	21	6	1.50	41
	-	71	79	17	4	2.00	33
	-	133	81	16	4	2.50	27

Fig. 8. Product distribution and current density over time for different reactor voltages and 1 M KOH as electrolyte.

4. Conclusion

The aim of this study was to demonstrate the transfer of electrochemical CO$_2$ reduction into continuous mode of operation at industrially relevant current density (CD) and to show how the reaction parameters, namely the electrolyte, are important tools to substantially improve performance. For that purpose, gas

diffusion electrodes (GDE) have been prepared via a dry deposition technique and loaded with carbon-supported SnO_2 nanoparticles. Their high dispersion and, thus, short diffusion lengths of the CO_2 molecules through the carbon network to the particle surface allows the achievable CD in the semi-batch experiments to be massively enhanced up to a value of 400 mA·cm^{-2} and 75% FE towards formate before mass transport limitation sets in. As this is one of the highest values reported in literature, it shows the potential and importance of GDE optimization in order to obtain industrially relevant reaction rates.

As for technical realization the process needs to be conducted in a continuous manner, the next step was to examine this mode of operation in a microstructured flow-cell. The transfer was shown to be successful in terms of product distribution and the CD range accessible. For the improvement of the substantially low energetic efficiency (EE), the electrolyte has been shown to play a pivotal role, as already suggested by other authors. Increasing concentration from 0.1 to 1 mol/L decreases ohmic losses due to higher conductivity but also improves intrinsic activity. Changing from $KHCO_3$ to KOH further improves the performance, in overall from an EE of below 10% to 41%, yet, at low CD. Higher CDs still necessitate relatively high reactor voltage and result in lower EE, e.g. ~30%, at 130 mA·cm^{-2} and FE of 80%. Necessary improvements would therefore comprise the further decrease of ohmic losses, also those not derived from electrolyte conductivity and to allow for even higher CD at low reactor voltage by improving the catalyst and by sophisticated GDE optimization which is one of the keys to come closer to technical application. Also long-term stability has yet to be demonstrated.

Acknowledgements

Symbols and abbreviations used

CCM		catalyst coated membrane
CD	[mA·cm^{-2}]	current density
E^0	[V]	standard potential
EE	[%]	energetic efficiency
FE	[%]	Faradaic efficiency
GDE		gas diffusion electrode
HER		hydrogen evolution reaction

References

[1]   C.H. Christensen, J. Rass-Hansen, C.C. Marsden, E. Taarning, K. Egeblad, *ChemSusChem* **2008** *1 (4)*, 283. DOI: 10.1002/cssc.200700168.

[2]   A.M. Appel, J.E. Bercaw, A.B. Bocarsly, H. Dobbek, D.L. DuBois, M. Dupuis, J.G. Ferry, E. Fujita, R. Hille, P.J.A. Kenis, C.A. Kerfeld, R.H. Morris, C.H.F. Peden, A.R. Portis, S.W. Ragsdale, T.B. Rauchfuss, J.N.H. Reek, L.C. Seefeldt, R.K. Thauer, G.L. Waldrop, *Chem. Rev.* **2013** *113 (8)*, 6621. DOI: 10.1021/cr300463y.

[3]   R. Agrawal, N.R. Singh, *Annual review of chemical and biomolecular engineering* **2010** *1*, 343. DOI: 10.1146/annurev-chembioeng-073009-100955.

[4]   G. Centi, S. Perathoner, *Catalysis Today* **2009** *148 (3-4)*, 191. DOI: 10.1016/j.cattod.2009.07.075.

[5]   M. Aresta, A. Dibenedetto, *Dalton Trans* **2007** *(28)*, 2975. DOI: 10.1039/b700658f.

[6]   C. Genovese, C. Ampelli, S. Perathoner, G. Centi, *Journal of Energy Chemistry* **2013** *22 (2)*, 202. DOI: 10.1016/S2095-4956(13)60026-1.

[7]   K.P. Kuhl, E.R. Cave, D.N. Abram, T.F. Jaramillo, *Energy Environ. Sci.* **2012** *5 (5)*, 7050. DOI: 10.1039/c2ee21234j.

[8]   Y. Hori, *Modern aspects of electrochemistry* **2008** *42*, 89. DOI: 10.1007/978-0-387-49489-0_3.

[9]   M. Azuma, K. Hashimoto, M. Hiramoto, M. Watanabe, T. Sakata, *J. Electrochem. Soc.* **1990** *137 (6)*, 1772. DOI: 10.1149/1.2086796.

[10]   A.S. Agarwal, Y. Zhai, D. Hill, N. Sridhar, *ChemSusChem* **2011** *4 (9)*, 1301. DOI: 10.1002/cssc.201100220.

[11]   C. Oloman, H. Li, *ChemSusChem* **2008** *1 (5)*, 385. DOI: 10.1002/cssc.200800015.

[12]   S. Enthaler, J. von Langermann, T. Schmidt, *Energy Environ. Sci.* **2010** *3 (9)*, 1207. DOI: 10.1039/b907569k.

[13]   B. Loges, A. Boddien, F. Gärtner, H. Junge, M. Beller, *Top Catal* **2010** *53 (13-14)*, 902. DOI: 10.1007/s11244-010-9522-8.

[14]   D.T. Whipple, P.J.A. Kenis, *J. Phys. Chem. Lett.* **2010** *1 (24)*, 3451. DOI: 10.1021/jz1012627.

[15]   H.-R.". Jhong, S. Ma, P.J.A. Kenis, *Current Opinion in Chemical Engineering* **2013** *2 (2)*, 191. DOI: 10.1016/j.coche.2013.03.005.

[16]   J. Rosen, G.S. Hutchings, Q. Lu, S. Rivera, Y. Zhou, D.G. Vlachos, F. Jiao, *ACS Catal.* **2015** *5 (7)*, 4293. DOI: 10.1021/acscatal.5b00840.

[17]   A.S. Varela, W. Ju, T. Reier, P. Strasser, *ACS Catal.* **2016**, 2136. DOI: 10.1021/acscatal.5b02550.

[18]   Q. Lu, J. Rosen, Y. Zhou, G.S. Hutchings, Y.C. Kimmel, J.G. Chen, F. Jiao, *Nat Comms* **2014** *5.* DOI: 10.1038/ncomms4242.

[19]   S. Zhang, P. Kang, T.J. Meyer, *J. Am. Chem. Soc.* **2014** *136 (5)*, 1734. DOI: 10.1021/ja4113885.

[20]   D.H. Won, C.H. Choi, J. Chung, M.W. Chung, E.-H. Kim, S.I. Woo, *ChemSusChem* **2015** *8 (18)*, 3092. DOI: 10.1002/cssc.201500694.

[21]   Q. Lu, J. Rosen, F. Jiao, *ChemCatChem* **2015** *7 (1)*, 38. DOI: 10.1002/cctc.201402669.

[22]   Y. Chen, C.W. Li, M.W. Kanan, *J. Am. Chem. Soc.* **2012** *134 (49)*, 19969. DOI: 10.1021/ja309317u.

[23] M. Asadi, B. Kumar, A. Behranginia, B.A. Rosen, A. Baskin, N. Repnin, D. Pisasale, P. Phillips, W. Zhu, R. Haasch, R.F. Klie, P. Král, J. Abiade, A. Salehi-Khojin, *Nat Comms* **2014** *5.* DOI: 10.1038/ncomms5470.

[24] S. Gao, X. Jiao, Z. Sun, W. Zhang, Y. Sun, C. Wang, Q. Hu, X. Zu, F. Yang, S. Yang, L. Liang, J. Wu, Y. Xie, *Angewandte Chemie (International ed. in English)* **2016** *55 (2)*, 698. DOI: 10.1002/anie.201509800.

[25] A. Dutta, A. Kuzume, M. Rahaman, S. Vesztergom, P. Broekmann, *ACS Catal.* **2015** *5 (12)*, 7498. DOI: 10.1021/acscatal.5b02322.

[26] M.F. Baruch, J.E. Pander, J.L. White, A.B. Bocarsly, *ACS Catal.* **2015** *5 (5)*, 3148. DOI: 10.1021/acscatal.5b00402.

[27] A. Martin Fernandez, G.O. Larrazábal, J. Perez-Ramirez, *Green Chem* **2015.** DOI: 10.1039/C5GC01893E.

[28] A. Del Castillo, M. Alvarez-Guerra, J. Solla-Gullón, A. Sáez, V. Montiel, A. Irabien, *Applied Energy* **2015** *157*, 165. DOI: 10.1016/j.apenergy.2015.08.012.

[29] M.N. Mahmood, D. Masheder, C.J. Harty, *J Appl Electrochem* **1987** *17 (6)*, 1159. DOI: 10.1007/BF01023599.

[30] N. Furuya, T. Yamazaki, M. Shibata, *Journal of Electroanalytical Chemistry* **1997** *431 (1)*, 39. DOI: 10.1016/S0022-0728(97)00159-9.

[31] D.T. Whipple, E.C. Finke, P.J.A. Kenis, *Electrochem. Solid-State Lett.* **2010** *13 (9)*, B109. DOI: 10.1149/1.3456590.

[32] D. Kopljar, A. Inan, P. Vindayer, R. Scholz, N. Frangos, N. Wagner, E. Klemm, *Chemie Ingenieur Technik* **2015** *87 (6)*, 855. DOI: 10.1002/cite.201400135.

[33] D. Kopljar, A. Inan, P. Vindayer, N. Wagner, E. Klemm, *J Appl Electrochem* **2014** *44 (10)*, 1107. DOI: 10.1007/s10800-014-0731-x.

[34] J. Wu, P.P. Sharma, B.H. Harris, X.-D. Zhou, *Journal of Power Sources* **2014** *258*, 189. DOI: 10.1016/j.jpowsour.2014.02.014.

[35] Q. Wang, H. Dong, H. Yu, H. Yu, *Journal of Power Sources* **2015** *279*, 1. DOI: 10.1016/j.jpowsour.2014.12.118.

[36] H.-R.". Jhong, F.R. Brushett, P.J.A. Kenis, *Adv. Energy Mater.* **2013** *3 (5)*, 589. DOI: 10.1002/aenm.201200759.

[37] K.C. Song, Y. Kang, *Materials Letters* **2000** *42 (5)*, 283. DOI: 10.1016/S0167-577X(99)00199-8.

[38] S. Lee, J.D. Ocon, Y.-i. Son, J. Lee, *J. Phys. Chem. C* **2015** *119 (9)*, 4884. DOI: 10.1021/jp512436w.

[39] H. Li, C. Oloman, *J Appl Electrochem* **2007** *37 (10)*, 1107. DOI: 10.1007/s10800-007-9371-8.

[40] K. Hara, A. Kudo, T. Sakata, *Journal of Electroanalytical Chemistry* **1995** *391 (1-2)*, 141. DOI: 10.1016/0022-0728(95)03935-A.

[41] C.H. Lee, M.W. Kanan, *ACS Catal.* **2015** *5 (1)*, 465. DOI: 10.1021/cs5017672.

[42]   Z.M. Detweiler, J.L. White, S.L. Bernasek, A.B. Bocarsly, *Langmuir* **2014** *30 (25)*, 7593. DOI: 10.1021/la501245p.

[43]   Y. Chen, M.W. Kanan, *J. Am. Chem. Soc.* **2012** *134 (4)*, 1986. DOI: 10.1021/ja2108799.

[44]   N. Wagner, M. Schulze, E. Gülzow, *Journal of Power Sources* **2004** *127 (1-2)*, 264. DOI: 10.1016/j.jpowsour.2003.09.022.

[45]   S. Ma, R. Luo, S. Moniri, Y. Lan, Kenis, P. J. A., *Journal of the Electrochemical Society* **2014** *161 (10)*, F1124–F1131. DOI: 10.1149/2.1201410jes.

[46]   E.J. Dufek, T.E. Lister, S.G. Stone, M.E. McIlwain, *Journal of the Electrochemical Society* **2012** *159 (9)*, F514–F517. DOI: 10.1149/2.011209jes.

[47]   J. Wu, F.G. Risalvato, F.-S. Ke, P.J. Pellechia, X.-D. Zhou, *Journal of the Electrochemical Society* **2012** *159 (7)*, F353–F359. DOI: 10.1149/2.049207jes.

[48]   M.R. Thorson, K.I. Siil, Kenis, P. J. A., *Journal of the Electrochemical Society* **2012** *160 (1)*, F69–F74. DOI: 10.1149/2.052301jes.

[49]   S. Verma, X. Lu, S. Ma, R.I. Masel, P.J.A. Kenis, *Physical chemistry chemical physics PCCP* **2015.** DOI: 10.1039/c5cp05665a.

Short text for the Tab. of contents section

Electrochemical reduction is an attractive pathway for its substantial utilization. This article describes how the important requirements of technical realization, namely high reaction rates, continuous operation and energetic efficiency are approached using gas diffusion electrodes loaded with electrocatalyst-nanoparticles, a microstructured flow-cell and electrolyte optimization.